AIAA 80-0419R

Numerical Simulation of the Wind Tunnel Environment by a Panel Method

K. D. Lee*
Boeing Commercial Airplane Company, Seattle, Wash.

A simulation technique has been developed to analyze the testing environment of practical three-dimensional subsonic wind tunnels. By using a higher-order panel method, the present technology can simulate interference effects due to various geometrical features that are ignored in most previously published approaches. Among them are the effects of the three-dimensional test sections, the finite test section length, the corner fillet, the model size and location, the model mounting system, and instrumentation. Results for different wind tunnel environments are presented to demonstrate their significance on the wind tunnel interference. The present technique provides a diagnostic tool for the interpretation of experimental data and an effective means for designing a test environment with minimum interference.

Nomenclature

a = slot spacing
AR = aspect ratio
B = boundary surface
b = wing semi-span
c = wing chord
C_D = potential flow drag coefficient
C_L = lift coefficient
C_M = pitching moment coefficient at the quarter chord
C_p = pressure coefficient
$dC_L/d\alpha$ = lift slope
h = tunnel semi-height
K = slotted-wall boundary condition coefficient, slot parameter
M_∞ = freestream Mach number
n = unit surface normal vector
r = distance in the compressibility coordinates
R = porous-wall boundary condition coefficient, porosity parameter
V_∞ = freestream velocity
v = perturbation velocity, $v=(\phi_x,\phi_y,\phi_z)$
w = perturbation mass flux, $w=(\beta^2\phi_x,\phi_y,\phi_z)$
W_n = normal mass flux, $W_n=(w+V_\infty)\cdot n$
x,y,z = coordinate system, see Fig. 3
α = model angle of attack, deg
β = compressibility parameter, $\beta^2=1-M_\infty^2$
δ = slot width
θ = flow angle
μ = doublet strength
σ = source strength
ϕ = perturbation potential

Introduction

ASSUMPTIONS used in classical wind tunnel wall interference theory are overly simplistic for analysis of many sources of interference effects in practical wind tunnels.[1] In the classical approaches, the disturbance due to the model is represented by simple singularities: a point vortex or a single horseshoe vortex for the lift and a doublet for the volume. Wind tunnel walls are treated as reflection planes where the wall boundary conditions are enforced for different cases of solid, porous and slotted walls. The tunnel wall interference at the model position is obtained from the influence of the image singularities due to tunnel walls. Such an approach is obviously incapable of simulating effects such as those due to complex model geometry, finite test section length, model mounting system, etc.

Several attempts have been made to investigate interference effects using modern computational technology and bypassing some of the earlier limiting assumptions. For example, lift interference was calculated using the vortex-lattice method in rectangular wind tunnels with ventilations of infinite length.[2,3] The effect of finite length of slots was investigated for lift interference in a square tunnel.[4] Transonic small disturbance equations were solved with slotted or porous wall boundary conditions.[5-7] So far, however, little progress has been made in simulating realistically the total testing environment of practical three-dimensional wind tunnels.

The objective of the present paper is to present and demonstrate a more complete numerical simulation technique using a higher-order panel method.[8] In the panel method, boundary surfaces of arbitrary geometry are simulated accurately. Hence, the present technology can simulate interference effects due to various geometrical features that are ignored in most previously published approaches. Among them are the effects of the three-dimensional test sections, the finite test section length, the corner fillet, the model size and location, the model mounting system, and instrumentation.

Improvements in the slotted-wall boundary conditions have been achieved theoretically and experimentally, leading to a better understanding of the slot performance.[9-11] The results are encouraging but still far from complete. An experimental study shows that the general form of the homogeneous slotted-wall boundary condition can be used once the boundary condition coefficients are determined experimentally.[12] In the present work, therefore, we used the classical linear, homogeneous slotted-wall boundary condition. The coefficient in the slotted-wall boundary condition is determined by correlation with experimental values rather than from the theories.[13]

The new simulation technique can model accurately the geometrical details of presently existing production tunnels. It also can accept the porous-wall boundary condition. Although it is a linear method, it provides an improvement in understanding the interference effects and sources associated with the actual testing environment in practical wind tunnels. Results are obtained for a lifting wing in a rectangular tunnel

Presented as Paper 80-0419 as the AIAA 11th Aerodynamic Testing Conference, Colorado Springs, Colo., March 18-20, 1980; submitted April 8, 1980; revision received Nov. 3, 1980.

*Specialist Engineer, Aerodynamics Research Unit. Member AIAA.

to evaluate the performance of slotted walls and the interference effects due to the finite test section length and the model mounting system.

Method of Solution

Governing Equation

The inviscid, irrotational flow is characterized by a perturbation velocity potential which satisfies

$$\beta^2 \frac{\partial^2 \phi}{\partial x^2} + \frac{\partial^2 \phi}{\partial y^2} + \frac{\partial^2 \phi}{\partial z^2} = 0 \tag{1}$$

Using the Goethert rule, Eq. (1) becomes the Laplace equation through a simple coordinate transformation. Green's theorem shows that any solution of the Laplace equation can be represented as a superposition of fundamental solutions. That is, the potential ϕ at the field point P can be expressed by the combined influence of source singularities of strength σ and doublet singularities of strength μ located at a point Q on the boundary surface B:

$$\phi(P) = \int\int_B \sigma(Q)\left(\frac{-1}{4\pi r}\right) dB + \int\int_B \mu(Q) \frac{\partial}{\partial n_Q}\left(\frac{1}{4\pi r}\right) dB \tag{2}$$

where r is the distance between the two points, P and Q, and $\partial / \partial n_Q$ is the derivative in the direction of the surface normal at the point Q.

In the higher-order panel method adopted for the calculations, the source strength is approximated as bilinear, while the doublet strength is taken to be biquadratic. On any solid surface, the basic boundary condition is that the total mass-flux vector is parallel to the surface:

$$W_n = (w + V_\infty) \cdot n = 0 \tag{3}$$

where w is the perturbation mass flux vector and n is the unit normal to the surface. The perturbation mass flux vector is given by

$$w = \left(\beta^2 \frac{\partial \phi}{\partial x}, \frac{\partial \phi}{\partial y}, \frac{\partial \phi}{\partial z}\right) \tag{4}$$

compared to the perturbation velocity which is

$$v = \left(\frac{\partial \phi}{\partial x}, \frac{\partial \phi}{\partial y}, \frac{\partial \phi}{\partial z}\right) \tag{5}$$

For a lifting body, the Kutta condition is satisfied at the trailing edge by defining a wake network and imposing the wake boundary condition.[8]

Slotted-Wall Boundary Condition

The flow characteristics at the slotted walls in the average sense can be approximated by the general form of the homogeneous-boundary condition:

$$C_p - C_{p_{\text{PLENUM}}} = 2K\alpha \frac{\partial \theta}{\partial x} + \frac{\beta}{R}\theta + \frac{\alpha^2 \theta^2}{\delta^2} \tag{6}$$

where θ is the flow angle in the tunnel near the wall. The length scales δ and α are related to the slot width and the slot spacing. The boundary condition coefficients, K and R, are the slot parameter and the porosity parameter, respectively, of the ventilated walls. The small perturbation approximation yields the following relations for the pressure coefficient and the flow angle:

$$C_p = -2\frac{\partial \phi}{\partial x} \tag{7}$$

$$\theta = \frac{\partial \phi}{\partial n} \tag{8}$$

The left-hand side of Eq. (6) is the pressure difference between the tunnel and the plenum. The right-hand side consists of three contributions, the first being the classical streamline curvature effect proportional to $\partial\theta/\partial x$, the second representing the viscous effect proportional to θ, and the third being a cross-flow effect proportional to θ^2.

In the present work, the plenum pressure is assumed to be the freestream static pressure. The nonlinear cross-flow effect is ignored to linearize the boundary condition, with the assumption that the flow angle at the slots is very small. The linear cross-flow term is also dropped since experimental results show no trace of the viscous effect, contrary to the claim in the early literature.[12,14] Therefore, the slotted-wall boundary condition becomes

$$\frac{\partial \phi}{\partial x} + K\alpha \frac{\partial}{\partial x}\left(\frac{\partial \phi}{\partial n}\right) = 0 \tag{9}$$

which is the form of the ideal slotted-wall boundary condition. The slotted-wall boundary condition coefficient K, however, is determined in the present work from experimental correlations.

The homogeneous boundary condition, Eq. (9), is integrated in order to make it acceptable to the panel program. Upon integration it becomes

$$(\phi - \phi_0) + K\alpha\left[\left(\frac{\partial \phi}{\partial n}\right) - \left(\frac{\partial \phi}{\partial n}\right)_0\right] = 0 \tag{10}$$

where the integration constants, subscript 0, refer to quantities at the beginning of the slotted section.

Wind Tunnel Modeling

An interior-flow problem is formulated inside the wind tunnel (Fig. 1). Wind tunnel walls, the model inside the test section, and other components like the model mounting system are approximated by networks of quadrilateral panels. Figure 2 shows the panel representation of a rectangular wind tunnel, with the strut and pitch assembly downstream of the test section. An "island" used as a means for model mounting can be seen protruding from the floor of the test section. Figure 3 shows the relative positions and paneling of a rectangular-wing model mounted on the island.

Depending on the boundary conditions, different types of singularities were distributed on the panels: doublet panels for the solid part of the tunnel walls and the wakes, source panels for the island and the strut and pitch assembly, and composite panels with sources and doublets for the lifting wing and the slotted walls of the test section. The total mass flux through the tunnel is conserved. In other words, the flux into the plenum is recovered back into the tunnel.

Results

Numerical solutions were obtained for several wind tunnel testing environments and compared with the solutions for unconfined, interference-free flow. A freestream Mach number of 0.5 was considered in a rectangular tunnel with a height-to-width ratio of two to three. The wind tunnel is assumed to have a constant cross section from the bellmouth to the diffuser. The model inside the tunnel is a rectangular

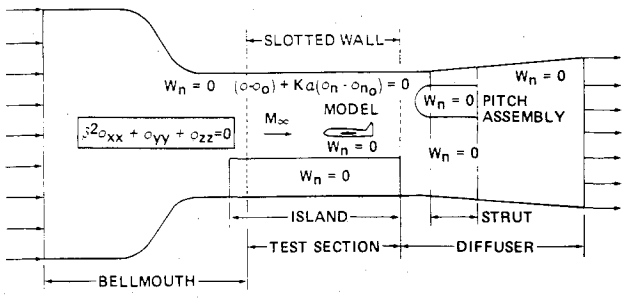

Fig. 1 Schematic formulation of problem.

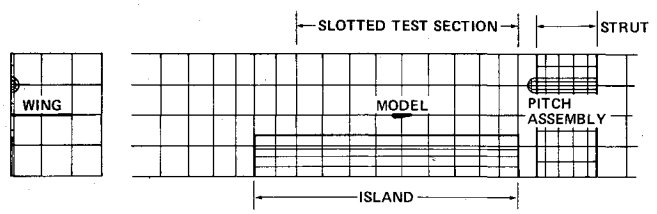

Fig. 2 Simulation of rectangular wind tunnel with strut and island.

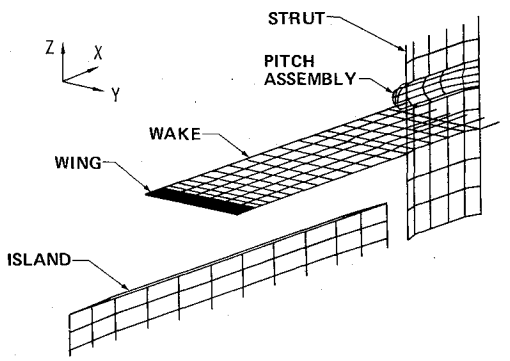

Fig. 3 Relative position: model and other components inside wind tunnel.

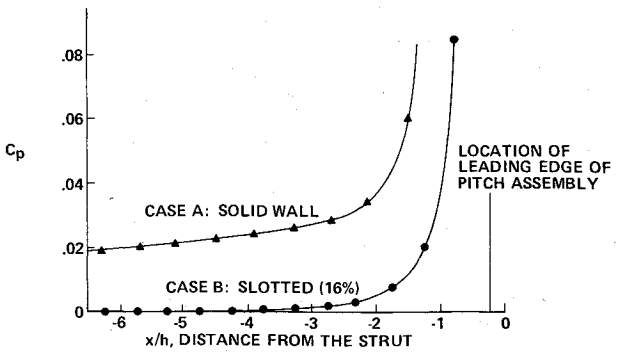

Fig. 4 Pressure distributions along centerline of empty tunnel—nonuniformity due to strut and pitch assembly ($M_\infty = 0.5$).

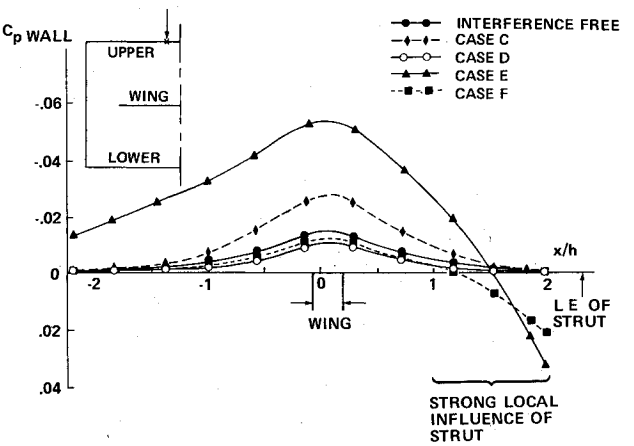

Fig. 5 Pressure distribution along upper wall of infinite test sections ($M_\infty = 0.5$, $\alpha = 0$).

lifting wing of $\mathcal{R} = 8$ with a constant, nonsymmetric airfoil section. The model spans two-thirds of the tunnel width.

Several tunnel variations explored are listed in Table 1. The slotted walls in the table are classified according to the length of the slots: infinite, semi-infinite, and finite. Infinite slots (case D) extend from upstream to downstream infinity. Semi-infinite slots (cases B and F) extend from upstream infinity to the downstream end of the test section which ends near the leading edge of the strut. Finite slots(cases G-J) extend a distance equal to about twice the height of the tunnel and end near the leading edge of the strut. In addition, case J is special in the sense that only the upper and side walls are slotted; the lower wall is everywhere solid. In all cases involving non infinite slots, the solid walls are imposed upstream and/or downstream of the slotted region.

The slotted-wall boundary condition coefficient K was obtained from Fig. 4 of Ref. 13 although the correlation may be valid only for two-dimensional tunnels. For example, the coefficient $K = 2.1$ is used for the wall openness ratio $\delta/\alpha = 0.12$ assuming that K is a dimensionless coefficient which depends only on the wall geometry.

The local interference effects were determined from calculations of the pressure distribution on the wing surface as well as at the tunnel walls. The normal mass-flux distribution at the wall position was also examined since it represents the change in the streamline curvature. Comparisons of the aerodynamic coefficients were made to determine the global interference effects.

Table 1 Wind tunnel configurations

Case	Type of tunnel walls	Slot openness, % Upper	Lower	Side	Model	Strut and pitch assembly	Island
A	Solid	0	0	0	No	Yes	No
B	Semi-infinite slots	16	16	16	No	Yes	No
C	Solid	0	0	0	Yes	No	No
D	Infinite slots	12	12	12	Yes	No	No
E	Solid	0	0	0	Yes	Yes	Yes
F	Semi-infinite slots	12	12	12	Yes	Yes	Yes
G	Finite slots	12	12	12	Yes	Yes	No
H	Finite slots	12	12	12	Yes	Yes	Yest
I	Finite slots	12	6	12	Yes	Yes	Yes
J	Finite slots with solid floor	12	0	12	Yes	Yes	Yes

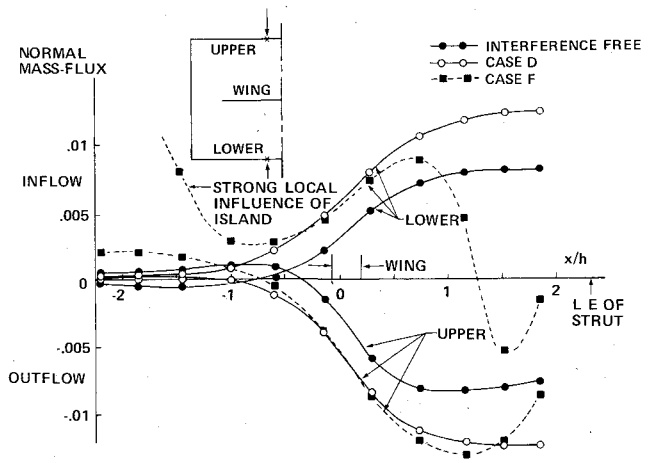

Fig. 6 Normal mass-flux distributions along slotted walls of infinite test sections ($M_\infty = 0.5$, $\alpha = 0$).

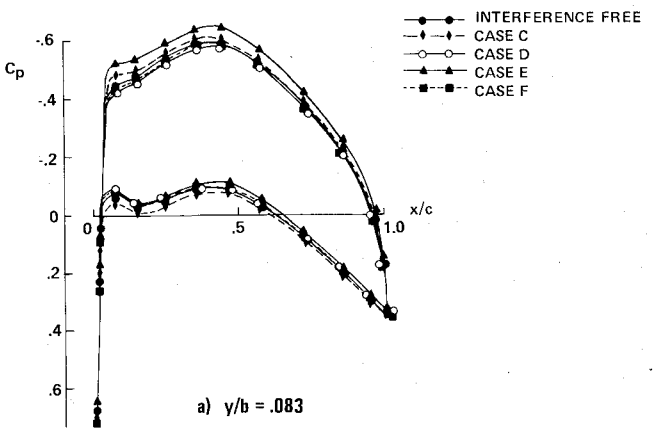

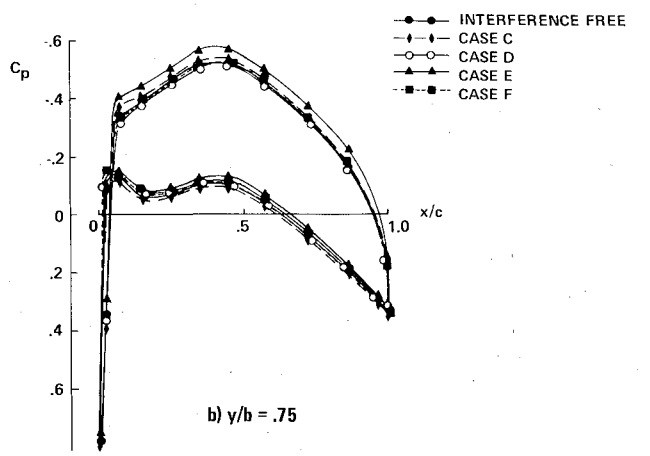

Fig. 7 Pressure distributions on wing surface ($M_\infty = 0.5$, $\alpha = 0$).

Empty Tunnel—Influence of Strut

Figure 4 shows the pressure distribution along the centerline of the empty tunnel containing only the strut and pitch assembly. Both solid and slotted walls were investigated. The effects of the strut and pitch assembly in the downstream region of the test section are very apparent. The maximum blockage ratio due to the strut and pitch assembly is 12.4% based on the tunnel cross-sectional area. Comparing the two curves, the blockage effect is seen to be less with the slotted walls. Slotted walls are also seen to reduce the buoyancy effect (i.e., the axial gradient of axial velocity) in the region normally occupied by a model.

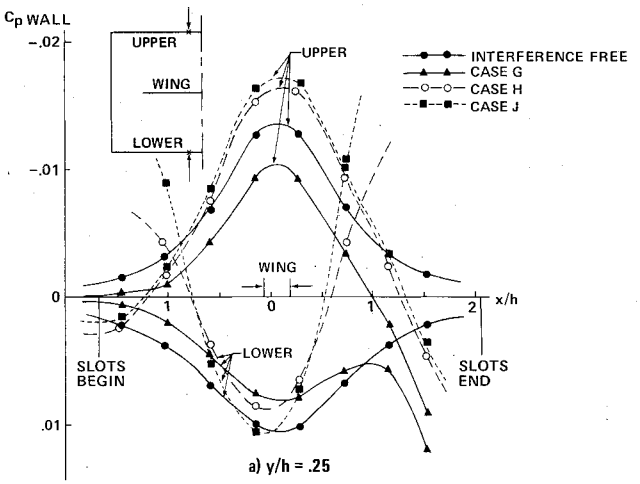

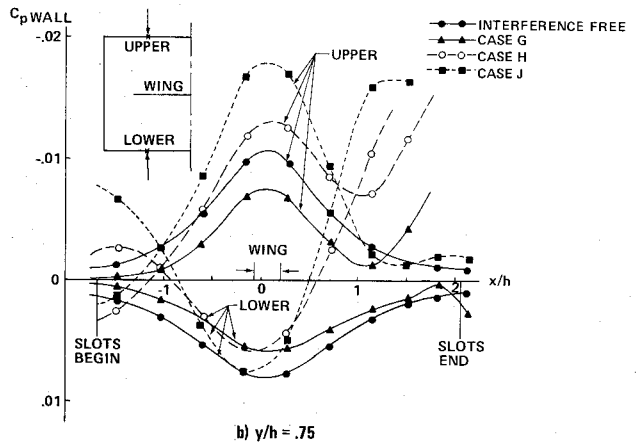

Fig. 8 Pressure distributions along tunnel walls with finite length of slots ($M_\infty = 0.5$, $\alpha = 0$).

Model in Tunnel—Influence of Mounting Systems and Slot Configurations

For the slotted walls, the semi-infinite slot configurations accompanied the installed strut and pitch assembly. Infinite slots were used when the strut was removed. Cases C and D compare the differences due to solid walls versus infinite slots for the case with the mounting systems (strut and island) removed. Cases E and F present similar comparisons with strut and island installed. For the latter cases, the pitch assembly is moved to the upper side of the strut and the model is mounted above the island as shown in Fig. 3. The maximum blockage ratio is about 6% for the strut and pitch assembly. It is 1.2% for the island but larger than that of the wing model. The top of the island extends to one-third of the test section height, which is close to the model.

Pressure and normal mass-flux distributions along the wind tunnel walls, Figs. 5 and 6, respectively, are compared for solid walls, slotted walls and interference-free flow. (The lateral location where the distributions are calculated is shown by the symbol X with an arrow in the insert appearing in the figures.) There patterns are quite similar to those predicted in the classical wind tunnel wall interference theory. Mass-flux distribution in the lower wall for case F demonstrates a strong local influence due to the island. The figures indicate that the slotted-wall wind tunnel with 12% openness is too open. The added presence of the island and the strut reduces this effect. Strong local interference is produced in the downstream region of the test section by the strut and pitch assembly.

The local interference effects on the wing pressure distribution are given in Fig. 7 and the global influence on aerodynamic coefficients is shown in Table 2, which again demonstrates that the slot openness ratio is too high. In Table

Table 2 Comparison of aerodynamic coefficients ($M_\infty = 0.5$, $\alpha = 0$, $\mathcal{R} = 8$)

Case	Tunnel specification	C_L	C_D	C_M
	Interference free	0.3616	0.0057	−0.1072
C	Solid walls without strut and island	0.3836 (0.3865)[a]	0.0044 (0.0042)	−0.1079 (−0.1077)
D	Infinite slots without strut and island	0.3510 (0.3554)	0.0063 (0.0061)	−0.1071 (−0.1072)
E	Solid walls with strut and island	0.3884	0.0047	−0.1099
F	Semi-infinite slots with strut and island	0.3524	0.0062	−0.1073

[a] ( ) values denote results from classical analytic solution.[1]

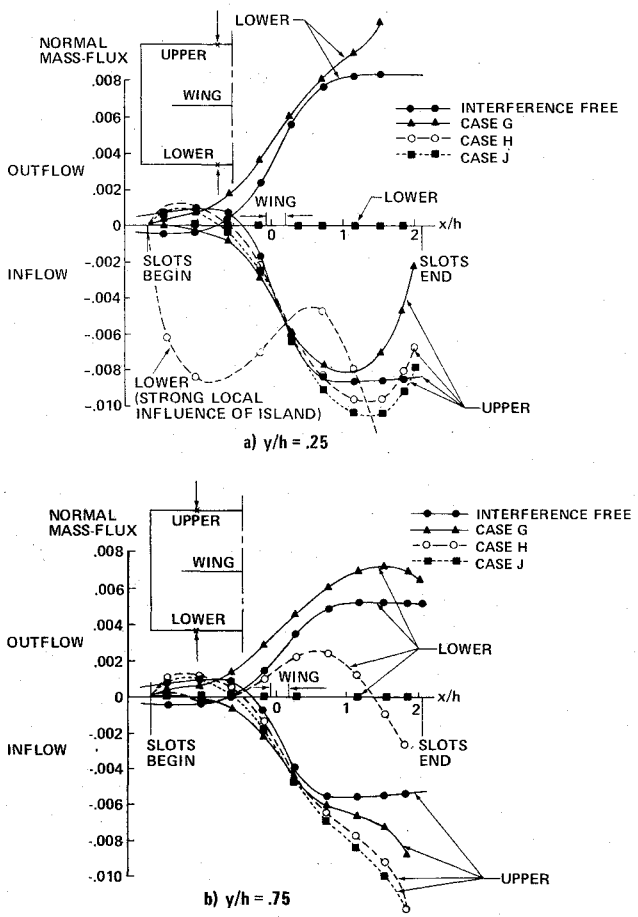

Fig. 9 Normal mass-flux distributions along tunnel walls with finite length of slots ($M_\infty = 0.5$, $\alpha = 0$).

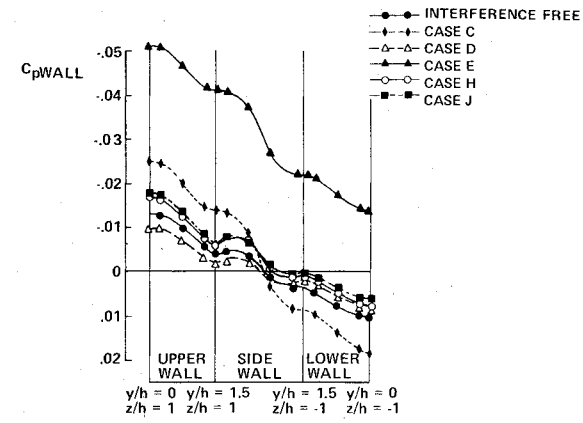

Fig. 10 Pressure distributions around tunnel wall at axial position, 0.105 h downstream from wing trailing edge ($M_\infty = 0.5$, $\alpha = 0$).

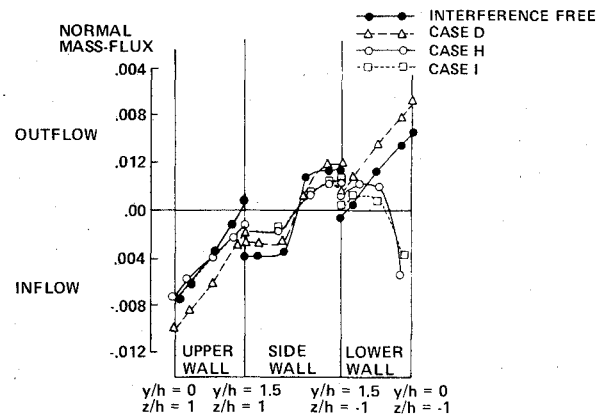

Fig. 11 Normal mass-flux distributions around tunnel wall at axial position 0.105 h downstream from wing trailing edge ($M_\infty = 0.5$, $\alpha = 0$).

2, results obtained from classical analytic solution of Ref. 1 are included in parentheses for comparison.

Finite Length of Slots—Influence of Mounting Systems

The effects of finite-slot length were considered for different cases of slotted tunnels. The length of slots in the test section is about twice the height of the tunnel. The island on the lower wall begins in front of the upstream end of the slots and extends downstream to the end of the slots, as shown in Fig. 2.

Figures 8 and 9 show pressure and normal mass-flux distributions at two different lateral stations along the upper and lower walls, for selected cases of tunnel configurations defined in Table 1. The effects of the island become more significant compared to the cases of infinite slots, producing large disturbances near the beginning and the end of slots. Comparisons between cases G and H also exhibit the strong local influence of the island. The case of a slotted tunnel with a solid floor (case J) is also compared in the figures.

Figure 10 shows pressure distributions plotted around the tunnel wall at an axial position downstream of the model trailing edge. The cases of finite slots are compared with the

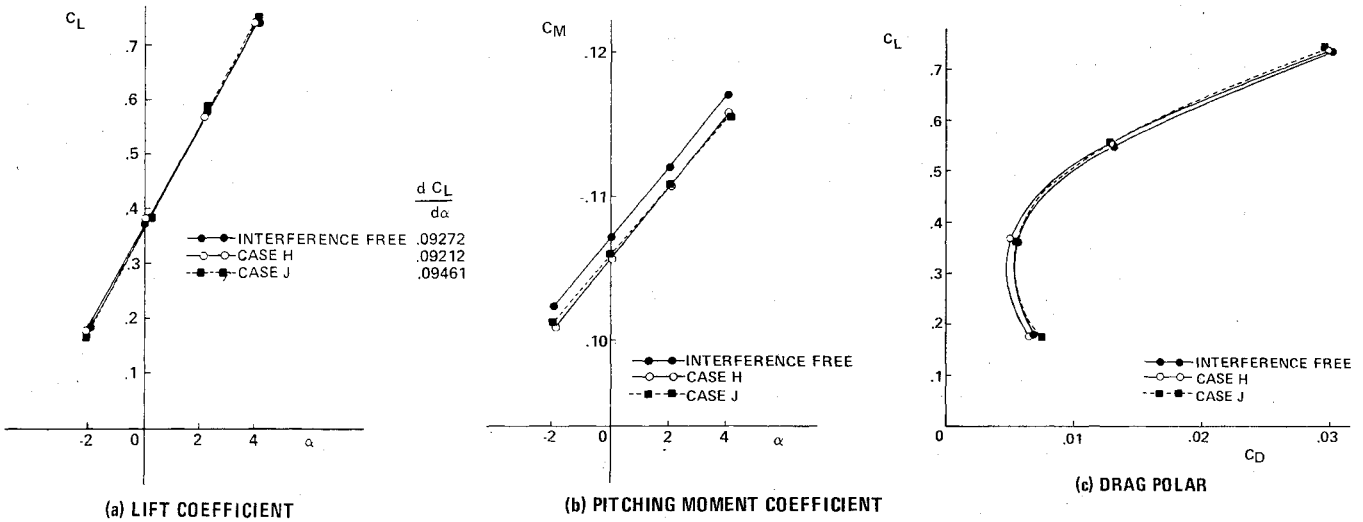

Fig. 12 Interference effects on aerodynamic coefficients ($M_\infty = 0.5$, $AR = 8$). a) Lift coefficient, b) pitching moment coefficient, c) drag polar.

cases of infinite walls without model mounting systems. The influence of the lift and the trailing vortices can be seen. The cases of clean tunnels (cases C and D) exhibit the trend predicted in the classical wall-interference theory. The slot openness ratio chosen seems to be too open in case D, but is not too open in the cases of finite slots (cases H and J). The presence of the island in the latter cases accelerates the flow inside the test section. The mass flux distributions around the tunnel wall are given in Fig. 11. The cases of finite slots with the model mounting systems (cases H and I) are compared with the case of infinite slots (case D) and the interference free flow. Case I does not produce much difference from case H except for the mass flux through the lower wall.

Aerodynamic Coefficients

In order to evaluate overall interference effects of the wind tunnel environment, aerodynamic forces and moments are considered for the cases of finite slots. Aerodynamic coefficients were computed by integrating the pressure distribution on the wing surface. Figure 12 shows the interference effects on aerodynamic coefficients. The lift-curve slope in the wind tunnel with a solid floor (case J) has about 2% error as compared with the interference free flow. While the interference effect on the magnitude of the lift is not significant, the pitching moment experiences more pronounced interference effects. The drag polar, Fig. 12c, exhibits large interference effects due to the wind tunnel environment.

Conclusions

The present approach for simulating the wind tunnel environment provides a more realistic and detailed insight into the multiple interference effects due to various sources in practical wind tunnels. Calculated results indicate that the interference effects are affected strongly by combinations of things which are usually ignored in the classical wall-interference theory. In the present investigation, strong interference effects are caused by the finite length of slots and by the fixtures inside the tunnel. Those effects not only change the tunnel flow conditions but also alter the slot performance.

The present simulation technique is a valuable diagnostic tool for the interpretation and reduction of experimental data, and provides an effective means for designing a testing environment with minimum interference effects. Another improvement in the simulation technique would be the inclusion of nonlinear effects at transonic speeds. This may be possible using the field panel method proposed recently in Ref. 15.

Acknowledgment

The author is indebted to Dr. Forrester T. Johnson for providing the computer code and helpful discussions.

References

[1] Pindzola, M. and Lo, C. F., "Boundary Interference at Subsonic Speeds in Wind Tunnels with Ventilated Walls," AEDC-TR-69-47, May 1969.

[2] Heltsley, F. L. and Dietz, W. E., Jr., "A Vortex Lattice Technique for Computing Ventilated Wind Tunnel Wall Interference," AEDC-TR-79-21, June 1979.

[3] Joppa, R. G., "A Method of Calculating Wind Tunnel Interference Factors for Tunnels of Arbitrary Cross-Section," NASA CR-845, July 1967.

[4] Ruger, C. and Baronti, P., "A Linear Solution of Lift Interference in Square Tunnels with Slotted Test Sections of Finite Length," NASA CR-144980, 1976.

[5] Newman, P. A. and Klunker, E. B., "Numerical Modeling of Tunnel-Wall and Body-Shape Effects on Transonic Flow over Finite Lifting Wings," NASA SP-347, 1975, pp. 1189-1212.

[6] Kraft, E. M. and Lo, C. F., "Analytical Determination of Blockage Effects in a Perforated-Wall Transonic Wind Tunnel," *AIAA Journal*, Vol. 15, April 1977, pp. 511-517.

[7] Kacprzynski, J. J., "Transonic Flowfield Past 2-D Airfoils Between Wind Tunnel Walls with Nonlinear Characteristics," *AIAA Journal*, Vol. 14, April 1976, pp. 533-535.

[8] Johnson, F. T., and Rubbert, P. E., "Advanced Panel-Type Influence Coefficient Methods Applied to Subsonic Flow," AIAA Paper 75-50, Jan. 1975.

[9] Barnwell, R. W., "Improvements in the Slotted-Wall Boundary Condition," *Proceedings of AIAA 9th Aerodynamic Testing Conference*, Arlington, Texas, June 1976.

[10] Berndt, S. B., "Inviscid Theory of Wall Interference in Slotted Test Sections," *AIAA Journal*, Vol. 15, Sept. 1977, pp. 1278-1287.

[11] Berndt, S. B., and Sörensen, H., "Flow Properties of Slotted Walls for Transonic Test Sections," *AGARD Conference Proceedings*, No. 174, Paper 17, Oct. 1975.

[12] Everhart, J. L. and Barnwell, R. W., "A Parametric Experimental Study of the Interference Effects and the Boundary-Condition Coefficient of Slotted Wind-Tunnel Walls," *Proceedings of AIAA 10th Aerodynamic Testing Conference*, San Diego, Calif., April 1978.

[13] Barnwell, R. W., "Design and Performance Evaluation of Slotted Walls for Two-Dimensional Wind Tunnels," NASA TM X-78648, Feb. 1978.

[14] Berndt, S. B., "Transonic Flow at a Slotted Test Section Wall," AFOSR TR 77-0035, Feb. 1977.

[15] Piers, W. J. and Sloof, J. W., "Calculation of Transonic Flow by Means of a Shock-Capturing Field Panel Method," *Proceedings, AIAA 4th Computational Fluid Dynamics Conference*, Williamsburg, Va., July 1979.